Phase segregation and nanoconfined fluid O_2 in a lithium-rich oxide cathode

Kit McColl[§#¶], Samuel W Coles[§#¶†], Pezhman Zarabadi-Poor[§#¶†], Benjamin J. Morgan[§#] and M. Saiful Islam[§#¶*]

[§]Department of Chemistry, University of Bath, Bath, UK
[#]The Faraday Institution, Harwell Science and Innovation Campus, Didcot, UK
[¶]Department of Materials, University of Oxford, Oxford, UK

*Corresponding author: km2083@bath.ac.uk, saiful.islam@materials.ox.ac.uk
[†]These authors contributed equally.

Abstract

Lithium-rich oxide cathodes lose energy density during cycling due to atomic disordering and nanoscale structural rearrangements, both of which are challenging to characterise. Here we use a combined approach of ab initio molecular dynamics and cluster-expansion-based Monte Carlo simulations to resolve the kinetics and thermodynamics of these processes in an exemplar layered Li-rich cathode, $Li_{1.2-x}Mn_{0.8}O_2$. We identify a kinetically accessible and thermodynamically favoured mechanism to form O_2 molecules in the bulk, involving Mn migration and driven by interlayer oxygen dimerisation. At the top of charge the bulk structure locally phase-segregates into MnO_2-rich regions and Mn-deficient nanovoids, which contain O_2 molecules as a nanoconfined fluid. These nanovoids are connected in a percolating network, potentially allowing long-ranged oxygen transport, and linking bulk O_2 formation to surface O_2 loss. These insights highlight the importance of future strategies to kinetically stabilise the bulk structure of Li-rich O-redox cathodes to maintain their high energy densities.

1. Introduction

Lithium-ion batteries using conventional cathodes based upon layered $LiCoO_2$ have revolutionised portable electronics and electric vehicles. Yet the continuing demand for improved battery performance means further increases in energy density are needed. Lithium-rich oxide cathodes offer higher energy densities than conventional cathodes because they utilize capacity from both transition metal and oxygen redox when cycled[1–3]. Oxygen-redox is typically accompanied by bulk structural changes that are associated with a large loss of energy density[4,5]. Understanding these structural changes and their relationship to O-redox behaviour is one of the major challenges for improving Li-rich cathodes. While some aspects of these O-redox driven structural changes are understood, such as that they involve transition metal migration[6,7] and oxygen dimerisation[8,9], the atomic- to nano-scale picture remains incomplete, in part due to the challenges for experiment and modelling to characterise Li-rich cathodes and their O-redox behaviour during operation[10].

Electronic structure modelling is a powerful tool for understanding atomic-level structures and predicting redox behaviour[11,12]. Modelling O-redox, however, is non-trivial[10,13]. Computational predictions of O-redox behaviour depend on the choice of structures used in these models. Because O-redox cathodes undergo atomic rearrangements during cycling, cathode structures after the early stages of the first charge are not known *a priori* and must be solved *in silico*. For computational modelling studies to make credible predictions of O-redox behaviour, both the kinetics and thermodynamics of structural rearrangements must be considered. Firstly, structural rearrangements must proceed via kinetically accessible paths. Secondly, any kinetically accessible structures should themselves be stable with respect to further rearrangement on relevant experimental timescales. Modelling schemes that predict behaviour from structures that form only via kinetically inaccessible pathways or from structures that are kinetically unstable can produce unrealistic

descriptions of O-redox. Finally, when modelling cathode behaviour after multiple cycles, thermodynamic considerations become more important. O-redox cathodes cycled towards a thermodynamic ground state exhibit crystallographic site disorder[14,15] and nanoscale structural changes, such as the formation of nanovoids[16–19]. To model disorder and nanoscale structural features, computational studies must search a vast configurational space to identify stable low-energy configurations and must use large enough cell sizes to capture the relevant structural features. Many models proposed to explain O-redox are based upon computational studies that have assessed structures using density functional theory (DFT)[20–30]. DFT, however, is too computationally expensive to directly investigate disorder and nanoscale structures, meaning that additional modelling methods are required to provide a complete picture of O-redox behaviour.

Here, we use a computational strategy that directly addresses these kinetic and thermodynamic factors in O-redox modelling. To identify kinetically viable atomic-scale rearrangements during the first charge, we have used long-timescale ab initio molecular dynamics (AIMD). In parallel, to account for disorder and nanoscale structural changes produced after many cycles, we have developed a DFT-derived cluster-expansion model of oxygen-redox, which we have used to perform large-scale Monte Carlo simulations. This approach allows us to efficiently search the vast configurational space for thermodynamically low-energy structures at the top of charge, and to conduct this search in structures containing ~50,000 atoms, so that nanoscale structural rearrangements can be examined.

We have applied this combined strategy to high-capacity O2-layered $Li_{1.2-x}Mn_{0.8}O_2$, which is an exemplar system for understanding Li-rich oxide cathodes. We identify a kinetically viable O-redox mechanism, in which the formation of transient interlayer superoxide and peroxide intermediates drives out-of-plane Mn migration, resulting in O_2 molecules forming within the bulk structure. The thermodynamic ground-state structure at the top of charge exhibits phase segregation into a two-phase mixture of MnO_2 and O_2. Bulk O_2 molecules are confined within nanometre-sized Mn-deficient voids that form a connected, percolating network. These O_2 molecules have a nanoconfined supercritical fluid character and can potentially diffuse through the network of voids, providing a mechanistic link between bulk O_2 formation and surface O_2 loss.

2. Results and discussion.

2.1 Kinetics of structural changes in charged O2–$Li_x[Li_{0.2}Mn_{0.8}]O_2$

The crystal structure of lithium-rich O2–$Li_{1.2}Mn_{0.8}O_2$ (Figure 1a) features O2-stacked[31] layers of octahedrally coordinated Li and Mn[32,33]. In the Mn-layers, a regular pattern of Li sites give a characteristic 'ribbon' superstructure[34]. Oxygen-ions are coordinated to either three (O–Mn_3) or two (O–Mn_2) Mn atoms; the O–Mn_2 atoms coordinate to the Li ions in the Mn-rich layers. These O–Mn_2 atoms have a single O 2p orbital at the top of the valence band that is unhybridised with any Mn 3d orbitals and is susceptible to oxidation upon charge[22,35].

To understand the first-cycle behaviour of O2–$Li_{1.2}Mn_{0.8}O_2$ in the oxygen-redox regime we modelled charging the pristine cathode structure past the conventional transition-metal redox limit (*i.e.*, Mn^{4+}) by removing one lithium ion per formula unit, giving a composition of $Li_{0.2}Mn_{0.8}O_2$. When relaxed using DFT, this delithiated structure appears stable with respect to structural rearrangement, with no observed Mn rearrangement or oxygen dimerisation (Figure 1b). The absence of rearrangements is an artefact of these DFT relaxations, with the structure trapped in a local minimum. The resulting delithiated structure, however, is unstable against structural rearrangement over experimental timescales[36,37].

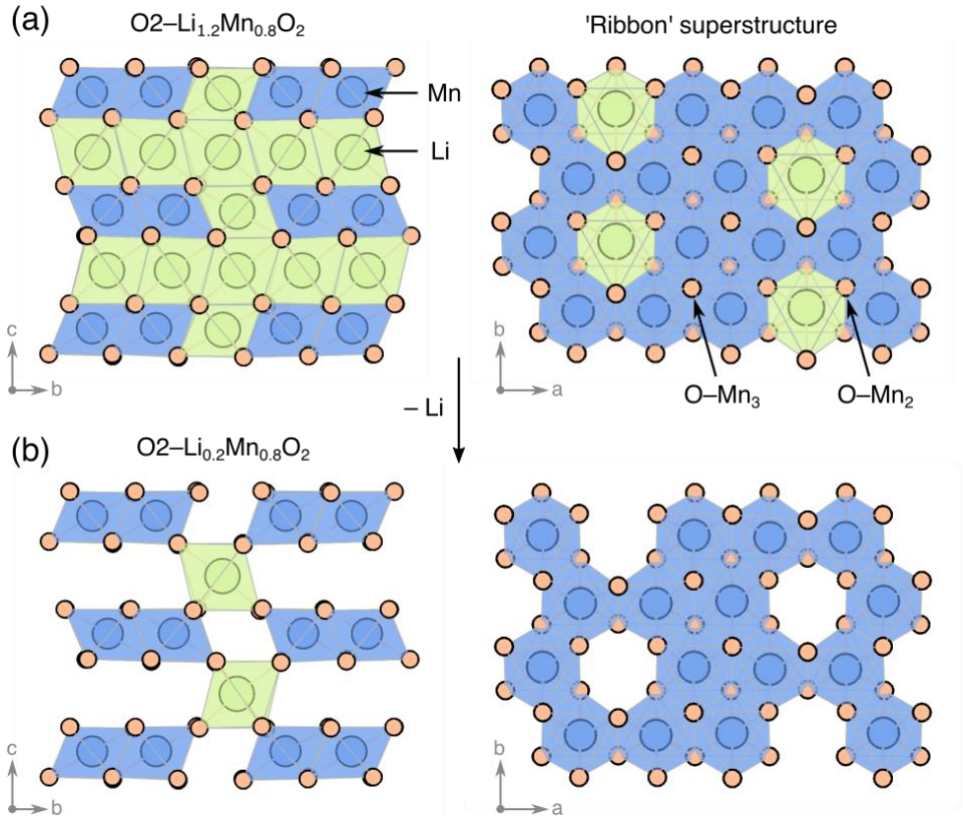

Figure 1. Structures of pristine O2–$Li_{1.2}Mn_{0.8}O_2$ and metastable O2–$Li_{0.2}Mn_{0.8}O_2$. (a) Pristine O2–$Li_{1.2}Mn_{0.8}O_2$ showing the octahedral interlayer Li sites, 'ribbon' superstructure arrangement of lithium ions in the Mn layer, and two different types of oxygen coordination: O–Mn_2 and O–Mn_3. (b) Metastable O2–$Li_{0.2}Mn_{0.8}O_2$ with the ribbon structure preserved, obtained without permitting host-framework rearrangements, showing octahedral lithium ions remaining in the Li layer only, in sites directly above and below the vacancies in the Mn-layers.

To identify kinetically accessible structural rearrangements, we replicated a thermal decomposition experiment using AIMD, by heating metastable $Li_{0.2}Mn_{0.8}O_2$ to 900 K and holding it at that temperature for 400 ps (Methods)[38,39]. For resulting structures displaying oxygen-dimerisation or transition metal ion migration, we performed full relaxations (quenching) with higher-accuracy hybrid DFT calculations to evaluate whether these rearrangements are thermodynamically favoured.

Applying this procedure to delithiated O2–$Li_{0.2}Mn_{0.8}O_2$ (Figure 2a) reveals a previously unreported O-redox mechanism. First, interlayer peroxide (O_2^{2-}) and superoxide (O_2^-) species form from O–Mn_2 atoms in adjacent transition-metal layers (Figure 2b&c, structure II). This drives Mn migration into the interlayer space, away from the O–O dimers, and results in de-coordination of the O–O dimers from the Mn to form a pair of O_2 molecules (structure III). Over longer timescales (~400 ps), more Mn ions migrate to the interlayer space, and more O_2 molecules form, which group together in the Mn-vacancy cluster (structure IV). This process is kinetically viable and causes an overall thermodynamic stabilisation of the system with structure IV approximately 11 eV/cell more stable than the starting structure I (Figure 2d).

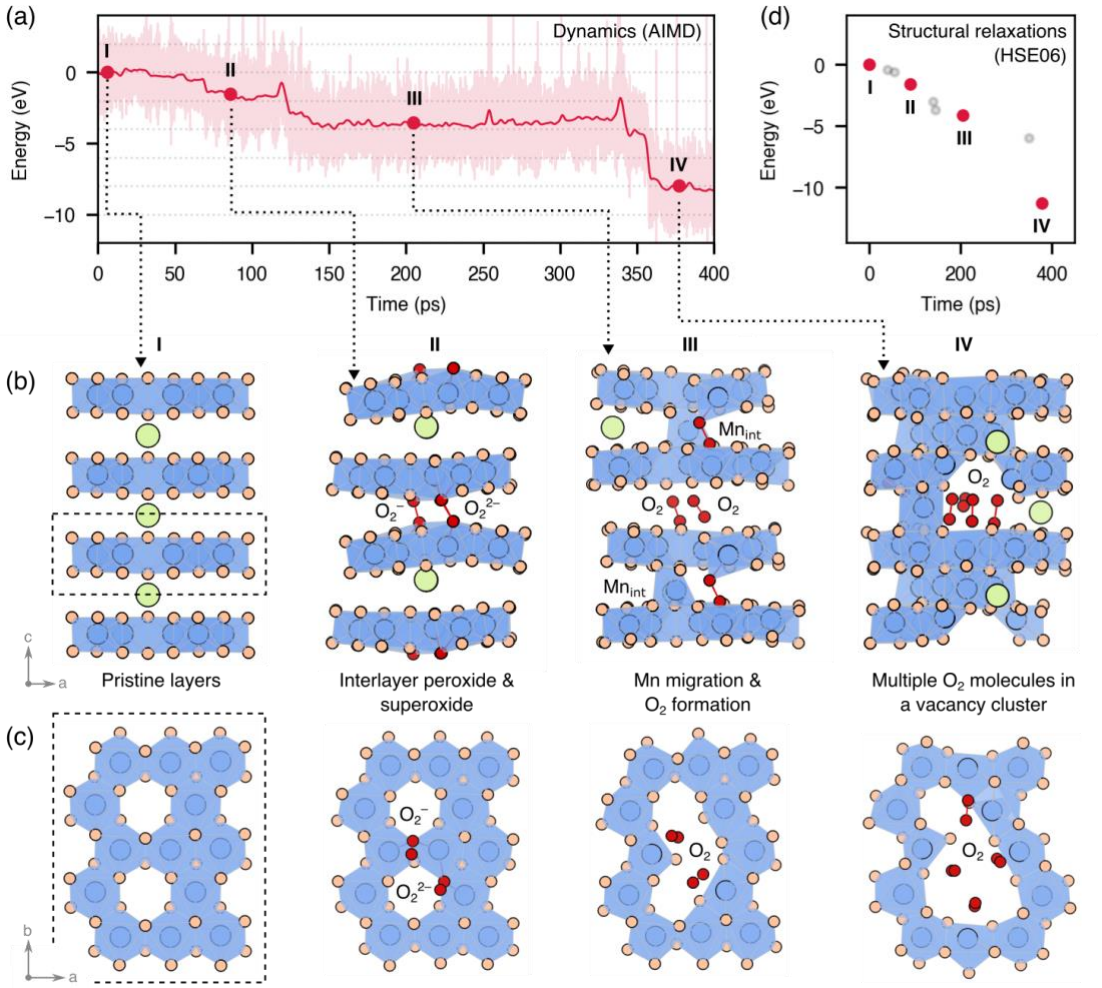

Figure 2. Mechanism of O–O dimerisation and Mn migration in $Li_{0.2}Mn_{0.8}O_2$ (a) Change in total energy from 400 ps DFT+*U* AIMD simulations at 900K, with indicated positions where some of the structures were extracted for further analysis. The shaded region shows the range of the fluctuations of total energy, and the red line indicates the energy averaged with a 1ps time window. (b) and (c) Optimised HSE06 equilibrium geometry of the extracted structures from (a) in both a/c and a/b planes. Some lithium ions have been removed for clarity. (d) Change in total energy for HSE06 geometry relaxations of structures **I** – **IV** plotted as a function of AIMD simulation time. Red circles correspond to the structures in (b) and (c), with grey circles indicating additional relaxed structures (Supplementary Information).

Previous studies have proposed an alternative pathway to forming O_2 in Li-rich layered cathodes, in which Mn migration occurs before oxygen dimerisation[24,29]. Our simulations show no evidence of this mechanism in $Li_{0.2}Mn_{0.8}O_2$. Indeed, our AIMD simulations always display interlayer O–O dimerisation before Mn migration (Figure S2). Mn migration to interlayer sites without accompanying oxygen dimerisation gives structures that are higher in energy than structures that contain interlayer superoxide and peroxide species (Figure S3). These results therefore indicate that the kinetically-favoured first step in the O-redox mechanism is interlayer O–O dimerisation, rather than Mn migration.

Transition metal migration and structural degradation in Li- and Mn-rich cathodes have previously been attributed to lattice strain between Li_2MnO_3 and $LiTMO_2$ domains[40] (where TM = Ni, Co). Our results, described here for the single-phase ribbon structured $Li_{1.2-x}Mn_{0.8}O_2$, suggest that there is a driving force for both transition metal migration into the Li layer and for structural degradation, irrespective of whether nanodomains are present. Structural degradation is initiated by oxidised framework O atoms and proceeds if the transition metal interlayer separation can contract to permit interlayer O–O dimerisation. Consequently, preventing interlayer O–O dimerisation is expected to improve the kinetic stability of the transition-metal layers against

rearrangement. This might be achieved by increasing the spacing between layers with “pillaring” cations or large interlayer ions, such as for Na-ion cathodes[41].

2.2 Mn-deficient nanovoids and O_2 confinement

The AIMD simulations investigate kinetically viable structural rearrangements during the first charge. To identify thermodynamically stable structures at the top-of-charge ($Mn_{0.8}O_2$), that are representative of the cathode after many cycles, while accounting for disorder and nanoscale structural changes, we developed a cluster expansion model of oxygen redox. For this cluster-expansion, we computed energies of structures along the along the O_2–MnO_2–MnO tie line using hybrid DFT. We considered two situations for the O_2 end-member: free gaseous O_2, which corresponds to oxygen lost from the cathode; and O_2 molecules confined in the bulk (Supplementary Notes 1,2). A convex-hull of formation energies, which defines the ground-state structures at a given composition, can be constructed for each of these two situations (Figure 3a). Structures at the top of charge ($Mn_{0.8}O_2$) are all above the ground-state hull connecting the O_2 states and MnO_2, indicating that $Mn_{0.8}O_2$ is metastable with respect to decomposition into a two-phase mixture of MnO_2 and O_2. The gaseous O_2 state is below the confined O_2 state, indicating that the lowest energy product is for O_2 to be lost from the system. $Mn_{0.8}O_2$ is also above the ground-state hull for the O_2 molecules confined in the bulk. This indicates that $Mn_{0.8}O_2$ is thermodynamically susceptible to decompose into MnO_2 and O_2 within the bulk, even if these O_2 molecules cannot be lost from the system.

To ensure accurate representation of the bulk structure, we fitted our cluster expansion using the energy of confined O_2. To systematically search for low-energy structures and examine nanoscale features, we used this cluster expansion model to run lattice Monte Carlo annealing simulations of structures containing 48,000 atoms, several orders of magnitude larger than is possible using pure DFT (Figure 3b). These simulations predict local phase-segregation type behaviour with the formation of MnO_2-rich regions and of Mn-deficient nanovoids containing confined O_2 molecules (Figure 3c). The phase-segregation also results in disorder, (Figure 3d), and a complete loss of the layered structure.

The O_2-filled voids vary in size with lengths from ~0.5 nm, to >1.5 nm. These voids form a 3D percolating network that connects 90 % to 95 % of O_2 molecules, which potentially permits O_2 transport through the cathode. The percolating network is highly tortuous, however, with a mean microscopic tortuosity factor (τ) of ~24, compared to $\tau = 1$ in the pristine structure[42]. The structure can be characterised as multiple large voids, filled with many O_2 molecules, often connected by narrow passages, that are likely to act as bottlenecks for any potential oxygen transport (Figure 3e&f).

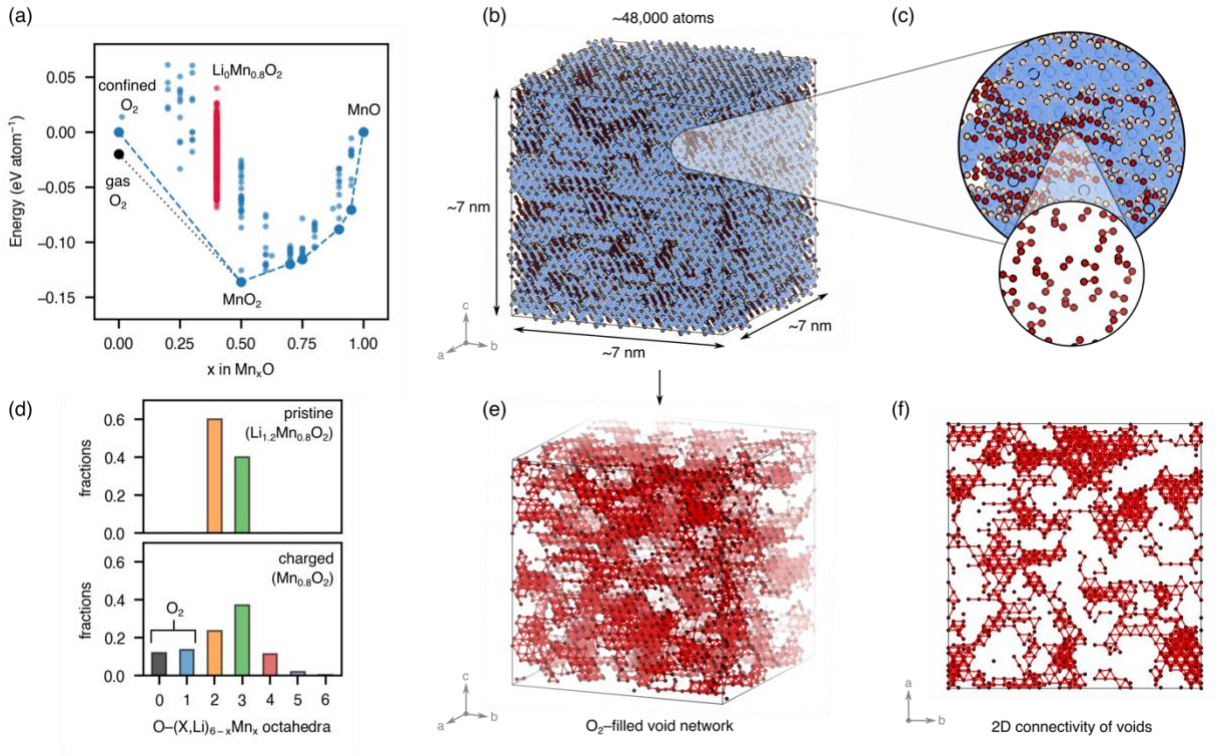

Figure 3. Local phase-segregation and formation of Mn-deficient, O_2-filled nanovoids at the top of charge. (a) DFT-calculated convex hull of formation energies used to fit the cluster expansion along the O_2–MnO_2–MnO tie line, showing the position of structures with the delithiated cathode composition ($Mn_{0.8}O_2$) above the ground-state hull. (b) Supercell of 48,000 atoms obtained from canonical Monte Carlo simulated annealing of $Mn_{0.8}O_2$. (c) Detailed structure of a section of the O_2-filled void network from (b). (d) Analysis of the O coordination environments in pristine $Li_{1.2}Mn_{0.8}O_2$ and delithiated $Mn_{0.8}O_2$ after charge. Approximately 25% of O atoms after cycling are those represented by O_2 molecules (*i.e.*, O–MnX_5 or O–X_6, where X is a vacancy) (Supplementary Note S1). (e) 3D representation of the void network, showing the O atoms in O_2 molecules only. (f) A 2D slide of the percolating void network, highlighting the bottlenecks between voids.

2.3 Dynamics of nanoconfined O_2 molecules

Having established that the cathode bulk structures at the top of charge feature nanovoids containing O_2 molecules, we performed additional molecular dynamics simulations at 300 K to characterise the dynamics of these O_2 molecules. The resulting radial distribution function (RDF) for Mn and lattice O^{2-} pairs shows sharp peaks, indicative of an ordered crystalline solid (Figure 4a). In contrast, the Mn–O_2 RDF shows broader peaks, with non-zero values inter-peak values, indicating that the molecular O_2 is mobile. A similar effect is seen in the RDF for the O atoms of only the O_2 molecules (Figure 4b). The second neighbour peak describes the O_2 inter-molecular distance. Instead of a sharp peak, as would be expected for solid crystalline O_2, the second peak is broad, indicating these O_2 molecules exhibit rotational and translational degrees of freedom.

The RDF for O_2 in the cathode bulk is compared to a simulated RDF of liquid O_2 (Fig. 4b). The cathode bulk O_2 has a second-neighbour peak maximum at a much smaller separation than for liquid O_2, and has a density of approximately 1.45 g cm^{-3}. This density is higher than that of liquid O_2 (1.141 g cm^{-3} at T = 88 K and ambient pressure), but lower than the density of solid β-O_2 (2.21 g cm^{-3} at T = 299 K and 5.5 GPa)[43]. The critical point for O_2 is at 154.6 K and 5.05 MPa, meaning that O_2 in the cathode bulk is predicted to be in the supercritical regime.

The mobile character of O_2 and presence of a percolating void network mean that the O_2 might diffuse through the structure. To probe possible O_2 transport, we ran AIMD on a $Li_{0.2}Mn_{0.8}O_2$ system with percolating Mn-void

pathways and containing six O_2 molecules (Figure 4d-f). Figure 4c shows the mean squared displacements (MSDs) for the O_2 molecules, lattice O^{2-} ions, and Li^+ ions in the system. The MSD for the lattice O^{2-} ions shows little change from the initial value of zero (Figure 4c), indicating that O^{2-} ions are not diffusing, as expected. In contrast, the MSDs for the O_2 molecules and Li^+ ions increase with time, indicating substantial diffusion of both species. The calculated diffusion coefficients for O_2 molecules and Li^+ ions are 1×10^{-7} cm^2 s^{-1} and ~7×10^{-8} cm^2 s^{-1} respectively, indicating that the oxygen molecules are highly mobile over this short length-scale. The non-crystalline diffusive character of this bulk O_2 indicates that these O_2 molecules can be considered a high-density nanoconfined fluid. Figures 4d-f show the positions of the O atoms from a single O_2 molecule over the course of the AIMD simulation. The molecule crosses the interlayer space and moves from one layer to beyond the layer above, demonstrating the potential for long-range O_2 diffusion give suitable void connectivity.

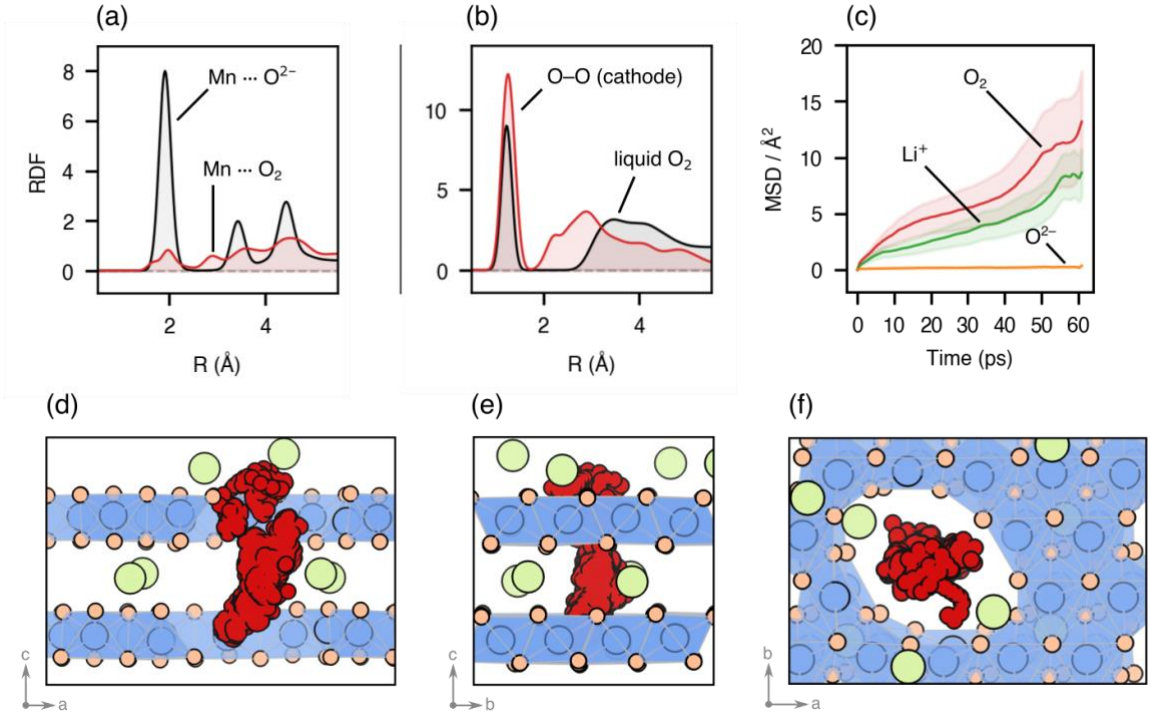

Figure 4. Transport and structural properties of O_2 molecules in nanovoids. (a) Radial distribution function (RDF) of Mn···O^{2-} and Mn···O_2 species in $Li_{0.2}Mn_{0.8}O_2$ from AIMD simulations showing solid character for the O^{2-} lattice, and fluid-like character for the O_2. (b) RDF of O···O species showing the compressed character of the O_2 in the cathode, relative to liquid O_2 at ambient pressure. (c) Mean squared displacement (MSD) of O_2 molecules show long-range diffusion. (d–f) Trajectory of a single O_2 molecule over 60ps, indicating that oxygen diffusion is possible through stacked voids in the layers. Red spheres show the position of the O atoms in the O_2 molecule every 200 fs.

2.4 Discussion and Outlook

The structural rearrangements that occur during cycling of Li-rich oxide cathodes introduce challenges for experimental characterisation and atomistic modelling of their O-redox behaviour. The previous absence of suitable modelling strategies to account for the kinetics and thermodynamics of these structural rearrangements[10] has resulted in uncertainty about the mechanisms of O-redox. Here, we have shown how a combination of AIMD and cluster expansion Monte Carlo can resolve these structural changes over the atomic and nanoscale, while accounting for both kinetics and thermodynamics.

Our results show that O_2 molecules can form in the bulk through kinetically accessible pathways. Peroxide and superoxide species form only as transient reaction intermediates along these pathways and are not the final O-redox product at the top of charge. This result is consistent with high-resolution resonant inelastic X-ray scattering (RIXS), neutron pair distribution function (PDF) and SQUID magnetometry measurements of several lithium-rich cathodes, which provide evidence for molecular O_2 confined in the bulk at the top of charge, and the absence of peroxide or superoxide species[34,41,44–48].

The convex hull of formation energies for Mn_xO_2 (Figure 3a) shows that there is a thermodynamic driving force at the top of charge for $Mn_{0.8}O_2$ to phase segregate into O_2 and MnO_2, regardless of whether the O_2 is lost from the system or confined in the bulk. O_2 loss and bulk O_2 formation therefore can be considered as different outcomes of the same thermodynamically-driven process whereby O^{2-} ions are oxidised to molecular O_2 [Ref [41]]. O_2 formed at the surface will be immediately lost. O_2 in the bulk is unstable with respect to outgassing and could contribute to net O_2 loss, but this is dependent upon diffusion of O_2 through the bulk material, and the permeability of the surface to O_2 molecules. On discharge, the bulk confined O_2 can be reduced to O^{2-}.

The idea that bulk O_2 formation and O_2 loss are outcomes of the same thermodynamically favoured process is likely to not be limited to $Li_xMn_{0.8}O_2$. If a material demonstrates oxygen loss as gas-phase O_2 this indicates a thermodynamic instability of the parent phase with respect to a two-phase mixture of O-deficient phase and molecular O_2. Providing the stabilisation energy to phase separate into this mixture is sufficiently large, molecular O_2 formation is likely to be thermodynamically favoured whether the resulting O_2 is confined in the bulk or released as a gas. This suggests that O_2 loss, which is widely observed in other Li-rich[14,49] and conventional layered oxides[50,51], may be an indication that these materials are also susceptible to bulk O_2 formation.

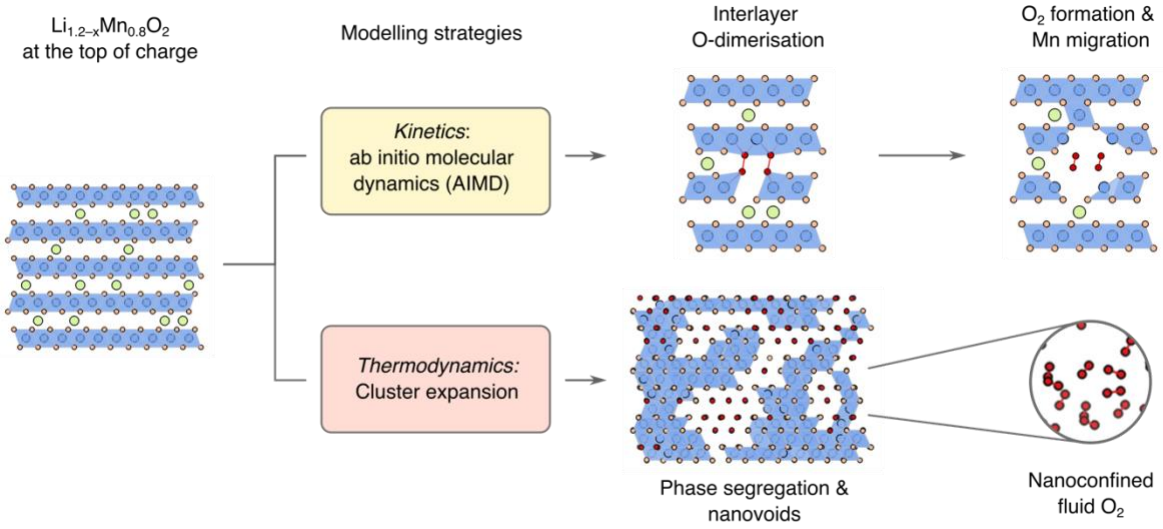

Figure 5. Schematic summary of the combined modelling strategies to probe structural rearrangements in delithiated O2–$Li_{1.2-x}Mn_{0.8}O_2$. At the top of charge, ribbon-superstructure $Li_{0.2}Mn_{0.8}O_2$ is predicted to be metastable by DFT structural relaxation but rearranges during experimental timescales. The kinetics and thermodynamics of these structural rearrangements can be modelled using ab initio molecular dynamics (AIMD) and cluster expansion Monte Carlo respectively. Modelling kinetic processes with AIMD and hybrid DFT relaxations identifies O-redox mechanism initiated by interlayer O–O dimerisation, forming stable O_2 molecules. Thermodynamic modelling using a cluster expansion model and Monte Carlo simulations identifies the formation of nano-scale voids containing O_2. AIMD characterises O_2 in the nanovoids as a high-density nanoconfined fluid.

Our study also explains experimentally observed disordering and nanostructuring driven by O-redox. Bulk confined O_2 cannot easily be directly imaged. Nevertheless, the phase segregation in our Monte Carlo simulations reveals that Mn-deficient nanovoids are a signature of bulk O_2 formation. This structural description

is consistent with observations of nanovoids in cycled cathodes from X-ray and neutron pair distribution function (PDF), small-angle X-ray and neutron scattering (SAXS, SANS), and electron microscopy experiments[16–19,52]. Some studies have attributed the formation of voids to the presence of oxygen vacancies, often in the context of oxygen loss[17]. Our results indicate voids can form even in the absence oxygen loss; oxygen atoms can instead dimerise to form molecular O_2 species near the vacated O sites. Our results also indicate that these voids can form throughout the $Li_{1.2-x}Mn_{0.8}O_2$ material; it is not necessary for them to first form at the surface and then penetrate into the bulk. Hence, design strategies to stabilise the bulk, as well as the surface, against the formation of nanovoids are expected to be important to prevent structural degradation and a loss of energy density.

Our large-scale models shine new light upon the properties of the confined O_2 molecules. Previous studies using ^{17}O NMR and AIMD have suggested that small numbers of O_2 molecules are rigidly caged within their local environment[44,53], with no long-range diffusion. Our results show a thermodynamic drive to form large voids that contain large numbers of O_2 molecules. Within the voids, these O_2 molecules are mobile, and collectively can be considered as a high-density supercritical nanoconfined fluid. Individual O_2 molecules in Mn-vacancy clusters may have a more solid-like character, but as the Mn-deficient voids increase in size, we predict that O_2 within these voids will display an increasingly fluid behaviour.

The fluid character of O_2 highlights important links between bulk O_2 formation, the cathode nanostructure, O_2 loss and voltage fade. Voltage fade has been associated with gradual O_2 loss from the bulk in oxide cathodes such as the lithium-rich nickel-manganese-cobalt (NMC) system at high states of charge, through a mechanism of oxygen vacancy transport from bulk to surface[54]. Our results suggest an alternative oxygen transport mechanism, in which fluid nanoconfined O_2 diffuses through a percolating network of voids. We calculate a local diffusion coefficient for nanoconfined O_2 of ~10^{-7} cm^2 s^{-1}.This calculated value is much higher than the macroscopic oxygen diffusion coefficient reported for Li-rich NMC (~10^{-17} cm^2 s^{-1})[54] from X-ray absorption and ptychography measurements. Long-range diffusion rates are therefore likely to be limited by other factors such as residual lithium in the structure, the high tortuosity and slow formation kinetics of the void network, and influenced by the variation in structure and composition of different Li-rich cathodes (Supplementary Note S3). Coatings and surface structures that prevent O_2 release from the bulk of cathode materials are potentially important to preserve long-term cycling stability, although these alone will not be able to inhibit structural rearrangements in the bulk where most of the O_2 is formed. Designing bulk structures with void networks that do not interconnect is also a possible strategy to inhibit oxygen transport and hence minimise oxygen loss from the surface.

In conclusion, the combination of ab initio molecular dynamics and cluster expansion allows the detailed atomic-scale exploration of a lithium-rich O-redox cathode, by resolving structures that are realistic representations of the charged cathode material. Using this approach, we have identified a thermodynamically-favoured and kinetically viable O-redox mechanism to form confined O_2 molecules in the bulk structure with Mn migration. Long-term cycling of the cathode results in local phase-segregation into MnO_2-rich regions and Mn-deficient nanovoids that contain O_2 molecules as a nanoconfined fluid. These nanovoids are connected in a percolating network, potentially allowing oxygen diffusion, which provides a link between bulk O_2 formation and O_2 loss through the surface. The combined methodology presented here answers longstanding questions about the atomic-to-nanoscale mechanisms of O-redox in Li-rich Mn-based cathodes, and highlights directions for improving the performance of other high energy density cathodes that display structural rearrangements during cycling.

1. Acknowledgements

The authors thank the Faraday Institution CATMAT project (EP/S003053/1, FIRG016) for financial support and the Michael high-performance computing (HPC) facility (FIRG030). This work made use of the UK's National Supercomputer, through the HEC Materials Chemistry Consortium (EP/R029431) and the Isambard UK National Tier-2 HPC Service (http://gw4.ac.uk/isambard/) operated by GW4 and the UK Met Office, funded by the EPSRC (EP/P020224/1). B.J.M. thanks the Royal Society for a fellowship (URF/R/191006). K.M. thanks Robert A. House (Oxford), Gregory J. Rees (Oxford), Andrey D. Poletayev (Oxford) and Alexander G. Squires (UCL) for valuable discussions.

2. Author contributions

3. Data availability

4. Conflicts of Interest

5. References

1. Zuo, W. *et al.* Li-rich cathodes for rechargeable Li-based batteries: reaction mechanisms and advanced characterization techniques. *Energy Env. Sci* **13**, 4450–4497 (2020).
2. Koga, H. *et al.* Reversible Oxygen Participation to the Redox Processes Revealed for $Li_{1.20}Mn_{0.54}Co_{0.13}Ni_{0.13}O_2$. *J. Electrochem. Soc.* **160**, A786–A792 (2013).
3. Sathiya, M. *et al.* Reversible anionic redox chemistry in high-capacity layered-oxide electrodes. *Nat. Mater.* **12**, 827–835 (2013).
4. Croy, J. R. *et al.* Examining Hysteresis in Composite $xLi_2MnO_3{\cdot}(1–x)LiMO_2$ Cathode Structures. *J. Phys. Chem. C* **117**, 6525–6536 (2013).
5. Gallagher, K. G. *et al.* Correlating hysteresis and voltage fade in lithium- and manganese-rich layered transition-metal oxide electrodes. *Electrochem. Commun.* **33**, 96–98 (2013).
6. Li, B. *et al.* Correlating ligand-to-metal charge transfer with voltage hysteresis in a Li-rich rock-salt compound exhibiting anionic redox. *Nat. Chem.* (2021) doi:10.1038/s41557-021-00775-2.
7. Gent, W. E. *et al.* Coupling between oxygen redox and cation migration explains unusual electrochemistry in lithium-rich layered oxides. *Nat. Commun.* **8**, 2091 (2017).
8. Hong, J. *et al.* Metal–oxygen decoordination stabilizes anion redox in Li-rich oxides. *Nat. Mater.* **18**, 256–265 (2019).
9. Gent, W. E., Abate, I. I., Yang, W., Nazar, L. F. & Chueh, W. C. Design Rules for High-Valent Redox in Intercalation Electrodes. *Joule* **4**, 1369–1397 (2020).
10. Zhang, M. *et al.* Pushing the limit of 3d transition metal-based layered oxides that use both cation and anion redox for energy storage. *Nat. Rev. Mater.* (2022) doi:10.1038/s41578-022-00416-1.
11. Urban, A., Seo, D.-H. & Ceder, G. Computational understanding of Li-ion batteries. *Npj Comput. Mater.* **2**, 16002 (2016).
12. Van der Ven, A., Deng, Z., Banerjee, S. & Ong, S. P. Rechargeable Alkali-Ion Battery Materials: Theory and Computation. *Chem. Rev.* **120**, 6977–7019 (2020).
13. Tygesen, A. S., Chang, J. H., Vegge, T. & García-Lastra, J. M. Computational framework for a systematic investigation of anionic redox process in Li-rich compounds. *Npj Comput. Mater.* **6**, 65 (2020).
14. Armstrong, A. R. *et al.* Demonstrating Oxygen Loss and Associated Structural Reorganization in the Lithium Battery Cathode $Li[Ni_{0.2}Li_{0.2}Mn_{0.6}]O_2$. *J. Am. Chem. Soc.* **128**, 8694–8698 (2006).
15. Zheng, J. *et al.* Structural and Chemical Evolution of Li- and Mn-Rich Layered Cathode Material. *Chem. Mater.* **27**, 1381–1390 (2015).
16. Hu, E. *et al.* Evolution of redox couples in Li- and Mn-rich cathode materials and mitigation of voltage fade by reducing oxygen release. *Nat. Energy* **3**, 690–698 (2018).
17. Yan, P. *et al.* Injection of oxygen vacancies in the bulk lattice of layered cathodes. *Nat. Nanotechnol.* **14**, 602–608 (2019).

18. Grenier, A. *et al.* Nanostructure Transformation as a Signature of Oxygen Redox in Li-Rich 3d and 4d Cathodes. *J. Am. Chem. Soc.* **143**, 5763–5770 (2021).

19. Zhao, E. *et al.* Quantifying the Anomalous Local and Nanostructure Evolutions Induced by Lattice Oxygen Redox in Lithium-Rich Cathodes. *Small Methods* **6**, 2200740 (2022).

20. Xie, Y., Saubanère, M. & Doublet, M.-L. Requirements for reversible extra-capacity in Li-rich layered oxides for Li-ion batteries. *Energy Env. Sci* **10**, 266–274 (2017).

21. Ben Yahia, M., Vergnet, J., Saubanère, M. & Doublet, M.-L. Unified picture of anionic redox in Li/Na-ion batteries. *Nat. Mater.* **18**, 496–502 (2019).

22. Seo, D.-H. *et al.* The structural and chemical origin of the oxygen redox activity in layered and cation-disordered Li-excess cathode materials. *Nat. Chem.* **8**, 692–697 (2016).

23. Okubo, M. & Yamada, A. Molecular Orbital Principles of Oxygen-Redox Battery Electrodes. *ACS Appl. Mater. Interfaces* **9**, 36463–36472 (2017).

24. Radin, M. D., Vinckeviciute, J., Seshadri, R. & Van der Ven, A. Manganese oxidation as the origin of the anomalous capacity of Mn-containing Li-excess cathode materials. *Nat. Energy* **4**, 639–646 (2019).

25. Saubanère, M., McCalla, E., Tarascon, J.-M. & Doublet, M.-L. The intriguing question of anionic redox in high-energy density cathodes for Li-ion batteries. *Energy Environ. Sci.* **9**, 984–991 (2016).

26. Chen, H. & Islam, M. S. Lithium Extraction Mechanism in Li-Rich Li_2MnO_3 Involving Oxygen Hole Formation and Dimerization. *Chem. Mater.* **28**, 6656–6663 (2016).

27. Lee, E. & Persson, K. A. Structural and Chemical Evolution of the Layered Li-Excess Li_xMnO_3 as a Function of Li Content from First-Principles Calculations. *Adv. Energy Mater.* **4**, 1400498 (2014).

28. Kim, B. *et al.* A theoretical framework for oxygen redox chemistry for sustainable batteries. *Nat. Sustain.* (2022) doi:10.1038/s41893-022-00890-z.

29. Vinckeviciute, J., Kitchaev, D. A. & Van der Ven, A. A Two-Step Oxidation Mechanism Controlled by Mn Migration Explains the First-Cycle Activation Behavior of Li_2MnO_3-Based Li-Excess Materials. *Chem. Mater.* **0**, null (0).

30. Kitchaev, D. A., Vinckeviciute, J. & Van der Ven, A. Delocalized Metal–Oxygen π-Redox Is the Origin of Anomalous Nonhysteretic Capacity in Li-Ion and Na-Ion Cathode Materials. *J. Am. Chem. Soc.* **143**, 1908–1916 (2021).

31. Delmas, C., Fouassier, C. & Hagenmuller, P. Structural classification and properties of the layered oxides. *Phys. BC* **99**, 81–85 (1980).

32. Eum, D. *et al.* Voltage decay and redox asymmetry mitigation by reversible cation migration in lithium-rich layered oxide electrodes. *Nat. Mater.* **19**, 419–427 (2020).

33. Cao, X. *et al.* Achieving stable anionic redox chemistry in Li-excess O2-type layered oxide cathode via chemical ion-exchange strategy. *Energy Storage Mater.* **38**, 1–8 (2021).

34. House, R. A. *et al.* Superstructure control of first-cycle voltage hysteresis in oxygen-redox cathodes. *Nature* **577**, 502–508 (2020).

35. Luo, K. *et al.* Charge-compensation in 3d-transition-metal-oxide intercalation cathodes through the generation of localized electron holes on oxygen. *Nat. Chem.* **8**, 684–691 (2016).

36. Eum, D. *et al.* Coupling structural evolution and oxygen-redox electrochemistry in layered transition metal oxides. *Nat. Mater.* **21**, 664–672 (2022).

37. House, R. A. *et al.* Delocalized electron holes on oxygen in a battery cathode. *Nat. Energy* (2023) doi:10.1038/s41560-023-01211-0.

38. Benedek, R. First-Cycle Simulation for Li-Rich Layered Oxide Cathode Material $x Li_2MnO_3 \cdot (1-x) LiMO_2$ (x= 0.4). *J. Electrochem. Soc.* **165**, A2667–A2674 (2018).

39. Zhang, Z., Zhao, S., Wang, B. & Yu, H. Local Redox Reaction of High Valence Manganese in Li_2MnO_3-Based Lithium Battery Cathodes. *Cell Rep. Phys. Sci.* **1**, 100061 (2020).

40. Liu, T. *et al.* Origin of structural degradation in Li-rich layered oxide cathode. *Nature* **606**, 305–312 (2022).

41. House, R. A. *et al.* The role of O_2 in O-redox cathodes for Li-ion batteries. *Nat. Energy* (2021) doi:10.1038/s41560-021-00780-2.

42. O'Rourke, C. & Morgan, B. J. crystal-torture: A crystal tortuosity module. *J. Open Source Softw.* **4**, 1306 (2019).

43. Freiman, Yu. A. & Jodl, H. J. Solid oxygen. *Phys. Rep.* **401**, 1–228 (2004).

44. House, R. A. *et al.* First-cycle voltage hysteresis in Li-rich 3d cathodes associated with molecular O_2 trapped in the bulk. *Nat. Energy* **5**, 777–785 (2020).

45. House, R. A. *et al.* Covalency does not suppress O_2 formation in 4d and 5d Li-rich O-redox cathodes. *Nat. Commun.* **12**, 2975 (2021).

46. House, R. A. *et al.* Detection of trapped molecular O_2 in a charged Li-rich cathode by Neutron PDF. *Energy Environ. Sci.* (2022) doi:10.1039/D1EE02237G.

47. McColl, K. *et al.* Transition metal migration and O_2 formation underpin voltage hysteresis in oxygen-redox disordered rocksalt cathodes. *Nat. Commun.* **13**, 5275 (2022).

48. Boivin, E. *et al.* Bulk O_2 formation and Mg displacement explain O-redox in $Na_{0.67}Mn_{0.72}Mg_{0.28}O_2$. *Joule* **5**, 1267–1280 (2021).

49. Lee, J. *et al.* Mitigating oxygen loss to improve the cycling performance of high capacity cation-disordered cathode materials. *Nat. Commun.* **8**, 981 (2017).

50. Jung, R., Metzger, M., Maglia, F., Stinner, C. & Gasteiger, H. A. Oxygen Release and Its Effect on the Cycling Stability of $LiNi_xMn_yCo_zO_2$ (NMC) Cathode Materials for Li-Ion Batteries. *J. Electrochem. Soc.* **164**, A1361 (2017).

51. Sharifi-Asl, S., Lu, J., Amine, K. & Shahbazian-Yassar, R. Oxygen Release Degradation in Li-Ion Battery Cathode Materials: Mechanisms and Mitigating Approaches. *Adv. Energy Mater.* **9**, 1900551 (2019).

52. Sun, C. *et al.* High-Voltage Cycling Induced Thermal Vulnerability in $LiCoO_2$ Cathode: Cation Loss and Oxygen Release Driven by Oxygen Vacancy Migration. *ACS Nano* **14**, 6181–6190 (2020).

53. Sharpe, R. *et al.* Redox Chemistry and the Role of Trapped Molecular O_2 in Li-Rich Disordered Rocksalt Oxyfluoride Cathodes. *J. Am. Chem. Soc.* **142**, 21799–21809 (2020).

54. Csernica, P. M. *et al.* Persistent and partially mobile oxygen vacancies in Li-rich layered oxides. *Nat. Energy* **6**, 642–652 (2021).